

Cite this: *RSC Sustainability*, 2024, 2, 153

# Construction of Pd–TiO<sub>x</sub> interfaces for selective hydrodeoxygenation of C=O bonds in vanillin by supporting Pd nanoparticles on ETS-10 zeolite<sup>†</sup>

Jianbin Huang,<sup>‡a</sup> Chang Zhou,<sup>‡a</sup> Jian Zhang,<sup>\*a</sup> Hao Meng,<sup>Ⓜb</sup> Shiyao Lu<sup>a</sup> and Feng-shou Xiao<sup>Ⓜ\*ab</sup>

The development of efficient catalysts for hydrodeoxygenation of vanillin to 5-methylguaiacol is highly desirable. Herein, we show a construction of Pd–TiO<sub>x</sub> interfaces by loading Pd nanoparticles on ETS-10 zeolite. These interfaces in the Pd/ETS-10 sample are quite efficient for the cleavage of C=O bonds in vanillin, exhibiting >99.9% vanillin conversion and 95.2% 5-methylguaiacol yield at 120 °C. Characterization and kinetic studies have confirmed that the unique Pd–TiO<sub>x</sub> interfaces activated the C=O bond of the intermediates in the reaction. This work might be helpful for the preparation of efficient catalysts for the hydrodeoxygenation of biomass-derived materials in the future.

Received 9th August 2023  
Accepted 2nd November 2023

DOI: 10.1039/d3su00271c

rsc.li/rscsus

## Sustainability spotlight

With the increasing demand for sustainable development, catalytic hydrodeoxygenation of lignin monomers to remove their aldehyde groups has garnered significant attention. Among the catalysts utilized for this process, TiO<sub>2</sub> supported metal catalysts have proven to be highly efficient, with particular emphasis on the metal–TiO<sub>x</sub> interfaces, which have been recognized as the active sites for catalysis. However, the catalytic performance of these metal/TiO<sub>x</sub> interfaces has been significantly limited due to the lack of oxygen vacancies on the bulky TiO<sub>2</sub> support. In this work, we report a construction of interfaces between Pd nanoparticles and subnanoscale TiO<sub>x</sub> chains by loading Pd nanoparticles on the ETS-10 zeolite crystals (Pd/ETS-10), where the formed Pd/TiO<sub>x</sub> interfaces are quite efficient for the selective removal of C=O bonds in hydrodeoxygenation of vanillin and vanillin-derivatives. Our work emphasizes the importance of the following UN sustainable development goals: sustainable and modern energy (SDG 7), sustainable production (SDG 12), and climate action (SDG 13).

## 1 Introduction

With the increasing demand for sustainable development, the utilization of biomass-derived materials has garnered significant attention.<sup>1–3</sup> Among these materials, lignin monomers such as vanillin and syringaldehyde have been regarded as promising substrates for the sustainable production of bio-fuels and aromatics.<sup>4–6</sup> Notably, there are unstable aldehydes or ketone groups in these molecules, hindering their utilization. Therefore, selective removal of aldehydes or ketone groups through catalytic hydrodeoxygenation is very important for the utilization of these biomass materials.<sup>7–10</sup> For example, the catalytic hydrodeoxygenation of the C=O bond in vanillin has been widely investigated.<sup>11–14</sup> Currently, it has been reported that TiO<sub>2</sub> supported metal catalysts are efficient for the

hydrodeoxygenation of biomass-based molecules.<sup>16,17</sup> For example, a TiO<sub>2</sub> supported ruthenium catalyst (Ru/TiO<sub>2</sub>) exhibited >95% toluene yield in the catalytic hydrodeoxygenation of *p*-cresol at 160 °C;<sup>15</sup> porous TiO<sub>2</sub> encapsulating Pd nanoparticles showed high hydrodeoxygenation selectivity for aromatic alcohols/aldehydes and phenolics while maintaining high catalytic activity;<sup>16</sup> a highly dispersed Pt/TiO<sub>2</sub> catalyst with a low metal loading was reported to be efficient in the upgrading of cotton straw derived bio-oil.<sup>17</sup> In these cases, it is found that the metal–TiO<sub>x</sub> interfaces such as Pd–TiO<sub>x</sub> interfaces are efficient for activation of the reactants, thus enhancing the catalytic activities.<sup>15–17</sup> Therefore, great efforts should be devoted to constructing unique metal–TiO<sub>x</sub> interfaces to achieve excellent performances in the hydrodeoxygenation of biomass-based compounds.<sup>18,19</sup>

Recently, strategies for constructing Pd–TiO<sub>x</sub> interfaces are focused on loading Pd nanoparticles on the specific facet of bulky TiO<sub>2</sub>, assembling a nanoscale structure with interaction between Pd and TiO<sub>2</sub>.<sup>20,21</sup> However, the lack of oxygen vacancies on the bulky TiO<sub>2</sub> limited the catalytic performance of these Pd/TiO<sub>2</sub> interfaces. Herein, we report the construction of interfaces between Pd nanoparticles and subnanoscale TiO<sub>x</sub> by loading Pd nanoparticles on ETS-10 zeolite crystals. ETS-10 is

<sup>a</sup>Beijing Advanced Innovation Center for Soft Matter, Science and Engineering, Beijing University of Chemical Technology, Beijing 100029, China. E-mail: jianzhangbuct@mail.buct.edu.cn; fsxiao@zju.edu.cn

<sup>b</sup>Key Lab of Biomass Chemical Engineering of Ministry of Education, College of Chemical and Biological Engineering, Zhejiang University, Hangzhou 310027, China

<sup>†</sup> Electronic supplementary information (ESI) available. See DOI: <https://doi.org/10.1039/d3su00271c>

<sup>‡</sup> These authors contributed equally.



a microporous titanasilicate zeolite which contains one-dimensional  $\text{TiO}_x$  nanowires with a sub-nanosized diameter crossing through the zeolite framework of the  $\text{SiO}_2$  matrix.<sup>22,23</sup> As expected, the unique Pd– $\text{TiO}_x$  interfaces in the Pd/ETS-10 sample are quite efficient for selective cleavage of C=O bonds in the hydrodeoxygenation of vanillin, an important lignin-derived biomass compound. Pd/ETS-10 exhibited >99.9% vanillin conversion and 95.2% 5-methylguaiacol yield at 120 °C.

## 2 Experimental

### 2.1 Materials

Sodium silicate solution (23.1 wt%  $\text{SiO}_2$  and 7.9 wt%  $\text{Na}_2\text{O}$ ), anatase ( $\text{TiO}_2$ , AR), and polyvinyl alcohol (PVA, MW 9000–10000) were purchased from Sigma-Aldrich Co. Sodium chloride (NaCl, AR), potassium chloride (KCl, AR), potassium fluoride (KF, AR), silica ( $\text{SiO}_2$ , quartz phase, AR), and sodium borohydride ( $\text{NaBH}_4$ , AR) were purchased from Sinopharm Chemical Reagent Co., Ltd. Rhodium(III) chloride ( $\text{RhCl}_3$ , AR), ruthenium(III) chloride ( $\text{RuCl}_3$ , AR), chloroplatinic acid ( $\text{H}_2\text{PtCl}_6$ , AR), chloroauric acid ( $\text{HAuCl}_4$ , AR), and palladium chloride ( $\text{PdCl}_2$ , AR) were bought from Beijing HWRK Chem Co. All chemicals were directly used without further purification.

### 2.2 Catalyst preparation

ETS-10 zeolite was synthesized as follows:<sup>22–25</sup> a titanium-silicate gel with a molar ratio of  $4.9\text{Na}_2\text{O}/1.5\text{K}_2\text{O}/1\text{TiO}_2/5.5\text{SiO}_2/136\text{H}_2\text{O}$  was prepared by mixing 7.188 g of sodium silicate solution, 7.289 g of  $\text{H}_2\text{O}$ , 0.43 g of KCl, 0.55 g of KF, 1.75 g of NaCl, and 0.4 g of anatase. The obtained titanium-silicate gel was hydrothermally treated at 200 °C for 3 days. ETS-10 zeolite was obtained by filtration, washing with a large amount of  $\text{H}_2\text{O}$ , and ion-exchange with acetic acid aqueous solution [1 g of ETS-10 with 51 mL of acetic acid solution (0.486 M)] at 50 °C for 4 h. Then, the Pd/ETS-10 catalyst was prepared by a sol-immobilization method as follows: 3.3 mg of  $\text{PdCl}_2$  and 3.0 mg of PVA were dissolved in 20 mL of  $\text{H}_2\text{O}$ . The obtained solution was kept stirring at 0 °C for 30 min, followed by addition of 0.94 mL of newly prepared  $\text{NaBH}_4$  aqueous solution (0.1 M). After stirring for 2 h, the Pd nanoparticle “solution” was mixed with 200 mg of ETS-10 zeolite. After stirring for another 3 h, the Pd/ETS-10 catalyst was obtained by filtration, washing with a large amount of  $\text{H}_2\text{O}$ , and drying at 80 °C overnight. Similarly, the Pt/ETS-10, Au/ETS-10, Ru/ETS-10, and Rh/ETS-10 catalysts were synthesized using  $\text{H}_2\text{PtCl}_6$ ,  $\text{HAuCl}_4$ ,  $\text{RuCl}_3$ , and  $\text{RhCl}_3$  as the metal precursors. Similarly, the Pd/ $\text{SiO}_2$  and Pd/ $\text{TiO}_2$  samples were prepared from  $\text{SiO}_2$  and  $\text{TiO}_2$  as the carriers.

### 2.3 Catalyst characterization

X-ray diffraction (XRD) patterns were obtained on a Rigaku D/MAX 2550 diffractometer with Cu  $K\alpha$  radiation ( $\lambda = 1.5418 \text{ \AA}$ ). Nitrogen-sorption isotherms were measured using a BELSORP-mini system. Before tests, the samples were treated at 100 °C overnight under vacuum conditions. Scanning electron microscopy (SEM) images were obtained on a Hitachi S-4800 electron microscope. Transmission electron microscopy (TEM)

measurements were performed on an FEI Tecnai G<sup>2</sup> F20 microscope. Metal contents were determined by inductively coupled plasma (ICP) analysis (PerkinElmer 3300DV). Ultraviolet and visible spectrophotometry (UV-vis) spectra were obtained on a Shimadzu UV3600PLUS spectrometer. Electron paramagnetic resonance (EPR) measurements were performed on a JEOL FA 200 operating at 9.70 GHz and –150 °C.

### 2.4 Catalytic tests

Catalytic hydrodeoxygenation of vanillin was performed in a steel autoclave equipped with a mechanical stirrer and a polytetrafluoroethylene (PTFE) bottle. After adding 1 g of vanillin, 0.2 g of catalyst, and 50 mL of  $\text{H}_2\text{O}$  (as a green solvent), the autoclave was sealed, purged with  $\text{H}_2$  4–5 times, and charged with 1 MPa of  $\text{H}_2$ . Then, the autoclave was heated to 120 °C and kept stirring for 1.5 h. After reaction, the catalyst was separated by filtration. The unreacted vanillin and products were extracted with 15 mL of ethyl acetate three times. The organic layers were combined and analyzed using a gas chromatograph equipped with a flame ionization (FID) detector and a HP-5 column. For the recyclability tests, the catalysts were separated by filtration after reaction, washing with a large amount of ethanol and ethyl acetate and drying under vacuum for the next run. The amounts of vanillin and water were reduced proportionally based on the amount of the used catalyst during the recyclability tests if a small amount of the catalyst was lost during the filtration process. In this manuscript, we measured turnover frequency (TOF) values based on the equation as follows:

$$\text{Turnover frequency (TOF)} = \frac{n_{\text{substrate}} \times \text{conversion}_{\text{substrate}}}{n_{\text{Pd}} \times \text{reaction time}} \quad (1)$$

where  $n_{\text{substrate}}$ ,  $\text{conversion}_{\text{substrate}}$ , and  $n_{\text{Pd}}$  stand for the moles of feeding vanillin substrate, the conversion of substrate, and moles of the total Pd species in the catalyst. The Pd loading was detected by ICP analysis. Reaction orders of vanillin and  $\text{H}_2$  were evaluated to study the structure–performance relationship of the Pd catalysts. The following reaction conditions were applied to make sure that the kinetic studies were evaluated within the kinetic regime (conversion <10%): for vanillyl alcohol reaction order: 200–350 mg of vanillyl alcohol, 1 mg of catalyst, 10 g of  $\text{H}_2\text{O}$ , 1 MPa of  $\text{H}_2$ , 120 °C, 0.17 h; for  $\text{H}_2$  reaction order: 200 mg of vanillyl alcohol, 1 mg of catalyst, 10 g of  $\text{H}_2\text{O}$ , 0.2–1 MPa of  $\text{H}_2$ , total pressure at 1 MPa, balanced with  $\text{N}_2$ , 120 °C, 0.17 h.

## 3 Results and discussion

### 3.1 Preparation of the Pd/ETS-10 catalyst

To construct efficient Pd– $\text{TiO}_x$  interfaces for C=O bond hydrodeoxygenation, Pd nanoparticles were loaded on ETS-10 zeolite with abundant  $\text{TiO}_x$  nanowires (Fig. S1†). The ETS-10 zeolite was synthesized from hydrothermal treatment of a titanium-silicate gel with a molar ratio of  $4.9\text{Na}_2\text{O}/1.5\text{K}_2\text{O}/1\text{TiO}_2/5.5\text{SiO}_2/136\text{H}_2\text{O}$ .<sup>22–24</sup> The as-obtained ETS-10 zeolite was ion-exchanged with acetic acid and supported Pd nanoparticles by a sol-



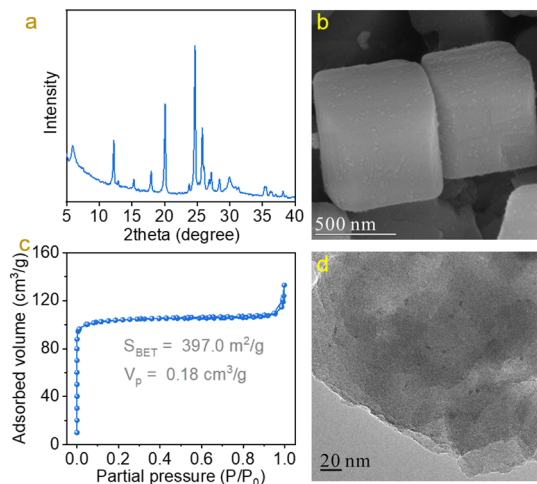


Fig. 1 (a) XRD pattern, (b) SEM image, (c)  $N_2$ -sorption isotherms, and (d) TEM image of the Pd/ETS-10 sample.

immobilization method to obtain the Pd/ETS-10 catalyst.<sup>26,27</sup> As shown in Fig. 1a, the Pd/ETS-10 sample exhibited typical characteristic peaks associated with ETS-10 zeolite,<sup>22–24</sup> where no peaks associated with Pd species could be observed in the XRD pattern, suggesting the high dispersion of Pd species (Fig. 1a). The SEM image was obtained to observe the morphology of the Pd/ETS-10 sample (Fig. 1b), giving polyhedral morphology, which was similar to that of ETS-10 zeolite in the literature.<sup>24,28</sup>  $N_2$ -sorption isotherms were recorded to study the surface area and pore volume of the Pd/ETS-10 sample. As shown in Fig. 1c, Pd/ETS-10 showed a steep step in the  $P/P_0 < 0.01$  region of the  $N_2$ -sorption isotherms, indicating the presence of microporosity in the sample. After calculation, the BET surface area ( $S_{BET}$ ) and pore volume ( $V_p$ ) are  $397.0 \text{ m}^2 \text{ g}^{-1}$  and  $0.18 \text{ cm}^3 \text{ g}^{-1}$ , respectively (Fig. 1c). TEM images were obtained to characterize the properties of Pd species. As shown in Fig. 1d, it can be clearly observed that Pd nanoparticles with mean size at 2.2 nm were uniformly dispersed on the ETS-10 zeolite (Fig. 1d and S2†). Based on the above characterization, it can be concluded that we have successfully synthesized the Pd/ETS-10 sample with high dispersion of Pd nanoparticles. For comparison, we have also synthesized ETS-10 zeolite supported Ru, Pt, Rh, and Au nanoparticles (Ru/ETS-10, Pt/ETS-10, Rh/ETS-10, and Au/ETS-10, Fig. S3 and Table S1†) and  $TiO_2$  and  $SiO_2$  supported Pd nanoparticles (Pd/ $TiO_2$  and Pd/ $SiO_2$ , Fig. S4–7†).

### 3.2 Catalytic performances in vanillin hydrodeoxygenation

The Pd/ETS-10 catalyst was applied in the hydrodeoxygenation of vanillin, which is a typical biomass conversion reaction (Fig. 2). As expected, the Pd/ETS-10 catalyst was efficient for the hydrodeoxygenation of vanillin. After catalysis at 120 °C for 1.5 h, the Pd/ETS-10 catalyst exhibited >99.9% vanillin conversion and 95.2% 5-methylguaiacol yield without any other products (Fig. 2). Even adjusting the catalytic temperature to 60 °C, the Pd/ETS-10 catalyst could still achieve >99.9% vanillin conversion and 93.0% 5-methylguaiacol yield after reaction for

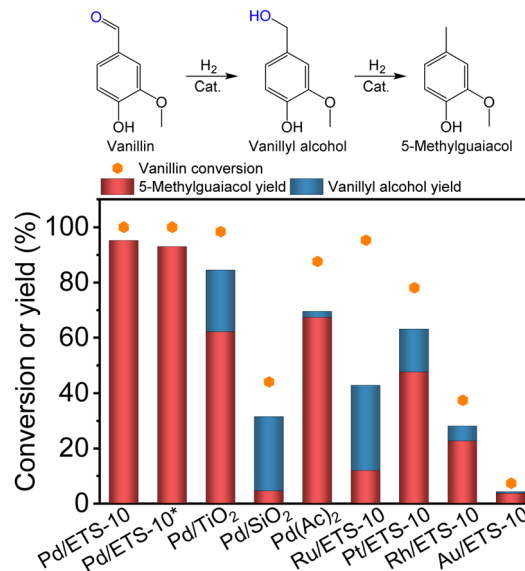


Fig. 2 Catalytic hydrodeoxygenation of vanillin over various catalysts. Typical reaction conditions: 1 g of vanillin, 0.2 g of catalyst, 50 g of  $H_2O$ , 1 MPa of  $H_2$ , 120 °C, 1.5 h. Reaction conditions for Pd/ETS-10\*: 152 mg of vanillin, 134.4 mg of catalyst, 10 g of  $H_2O$ , 2 MPa of  $H_2$ , 60 °C, 5 h.

5 h at a little lower substrate to catalyst ratio (Fig. 2), which is comparable to that reported previously (Table S2†).<sup>29–31</sup> These results suggest the positive role of the Pd– $TiO_x$  interfaces in the Pd/ETS-10 catalyst. In comparison, the referenced Pd/ $TiO_2$  catalyst could not achieve full vanillin conversion, giving vanillin conversion, vanillyl alcohol, and 5-methylguaiacol yields at 98.4%, 22.4%, and 62.1%, respectively (Fig. 2). Considering that the Pd/ $TiO_2$  catalyst also possessed Pd/ $TiO_x$  interfaces,<sup>21,32</sup> better catalytic performance over the Pd/ETS-10 than that of Pd/ $TiO_2$  indicates more positive effect of the unique Pd– $TiO_x$  interfaces in the Pd/ETS-10 than that of the normal Pd– $TiO_x$  interfaces in the Pd/ $TiO_2$ .

Considering that ETS-10 zeolite has  $SiO_2$  species, we have also synthesized Pd/ $SiO_2$  samples to exclude the effect of Pd/ $SiO_2$  interfaces on the hydrodeoxygenation. As shown in Fig. 2, the Pd/ $SiO_2$  catalyst showed vanillin conversion, vanillyl alcohol, and 5-methylguaiacol yields at 44.1%, 26.9%, and 4.5%, respectively, which are much lower than those of the Pd/ETS-10 catalyst (Fig. 2). Furthermore, we have also employed homogeneous Pd( $Ac$ )<sub>2</sub> for the hydrodeoxygenation of vanillin, exhibiting vanillin conversion, vanillyl alcohol, and 5-methylguaiacol yields at 87.6%, 2.2%, and 67.3%, respectively. Generally, homogeneous catalysts are more active than heterogeneous ones because of higher metal dispersion.<sup>33</sup> However, better catalytic performance of the heterogeneous Pd/ETS-10 than that of homogeneous Pd( $Ac$ )<sub>2</sub> confirmed again the positive role of the unique Pd– $TiO_x$  interfaces in the Pd/ETS-10 catalyst for the hydrodeoxygenation.

Furthermore, we also tested the catalytic performance of Pd/ETS-10 for the cleavage of C–O bonds directly connected with the benzene ring. As shown in Fig. S8,† the Pd/ETS-10 catalyst was completely inactive for the catalytic hydrodeoxygenation of



both phenol and anisole. These results indicate the selective hydrodeoxygenation of the C=O bonds rather than C–O bonds connected with the benzene ring for vanillin or vanillin derivatives over the Pd/ETS-10 catalyst.

Moreover, we tested the catalytic performances of the ETS-10 zeolite supported Ru, Pt, Rh, and Au nanoparticles (Ru/ETS-10, Pt/ETS-10, Rh/ETS-10, and Au/ETS-10, Fig. S3†). The Ru/ETS-10, Pt/ETS-10, Rh/ETS-10, and Au/ETS-10 catalysts exhibited 5-methylguaiacol yields at 11.9%, 47.6%, 22.6%, and 3.6%, respectively (Fig. 2), which are much lower than that of the Pd/ETS-10. These results demonstrate the unique catalytic hydrodeoxygenation ability of the Pd–TiO<sub>x</sub> interfaces in Pd/ETS-10.

### 3.3 Structure–performance relationship

To investigate the origin of the excellent catalytic properties in the hydrodeoxygenation of vanillin over the Pd/ETS-10 catalyst, the key step should be pursued. The hydrodeoxygenation of vanillin includes hydrogenation of the aldehyde group to the alcohol group and deoxygenation of the alcohol group to the methyl group.<sup>29–31</sup> Therefore, vanillin and vanillyl alcohol were applied as the probe substrates of the kinetic studies. As shown in Fig. S9,† Pd/ETS-10 displayed vanillin and vanillyl alcohol conversion rates at 792.7 and 102.2 min<sup>−1</sup>. The relatively higher vanillin conversion rate suggests that the cleavage of the C–O bond without connection of the benzene ring rather than the conversion of C=O into C–O bonds is the key step in the hydrodeoxygenation of vanillin. A similar trend was also observed over the Pd/TiO<sub>2</sub> catalyst, which exhibited vanillin and vanillyl alcohol conversion rates at 223.1 and 60.8 min<sup>−1</sup> (Fig. S9†). This phenomenon is in accordance with the activation energies of the Pd catalysts. As shown in Fig. S10,† we tested the activation energy of vanillin and vanillyl alcohol over the Pd/ETS-10 and Pd/TiO<sub>2</sub> catalysts to compare the catalytic activities of the two catalysts. The activation energy values of vanillin over the Pd/ETS-10 or Pd/TiO<sub>2</sub> catalysts are lower than those of vanillyl alcohol over the Pd/ETS-10 or Pd/TiO<sub>2</sub> catalysts, indicating that the activation of the vanillyl alcohol molecule is more difficult than that of vanillin in the hydrodeoxygenation. The activation energy (116.6 ± 4.5 kJ mol<sup>−1</sup>) of vanillyl alcohol over Pd/TiO<sub>2</sub> is significantly higher than that (76.1 ± 6.6 kJ mol<sup>−1</sup>) of vanillyl alcohol over Pd/ETS-10 (Fig. S10†),

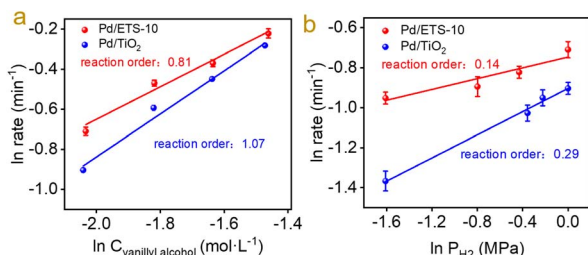


Fig. 3 Reaction order of (a) vanillyl alcohol and (b) H<sub>2</sub> over the Pd/ETS-10 and Pd/TiO<sub>2</sub> catalysts. Reaction conditions for vanillyl alcohol reaction order: 200–350 mg of vanillyl alcohol, 1 mg of catalyst, 10 g of H<sub>2</sub>O, 1 MPa of H<sub>2</sub>, 120 °C, 0.17 h. Reaction conditions for H<sub>2</sub> reaction order: 200 mg of vanillyl alcohol, 1 mg of catalyst, 10 g of H<sub>2</sub>O, 0.2–1 MPa of H<sub>2</sub>, total pressure at 1 MPa, balanced with N<sub>2</sub>, 120 °C, 0.17 h.

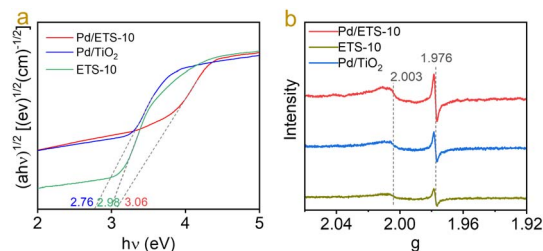


Fig. 4 (a) UV-visible diffuse reflectance spectra of the ETS-10, Pd/ETS-10, and Pd/TiO<sub>2</sub> catalysts; (b) EPR spectra of the ETS-10, Pd/ETS-10, and Pd/TiO<sub>2</sub> catalysts.

indicating stronger ability of Pd/ETS-10 than that of Pd/TiO<sub>2</sub> for the activation of the C–O bond. Furthermore, we measured the reaction orders for hydrodeoxygenation of vanillyl alcohol, as shown in Fig. 3. Notably, Pd/ETS-10 has vanillyl alcohol and H<sub>2</sub> orders at 0.81 and 0.14 (Fig. 3), indicating that the activation of the vanillyl alcohol molecule is more difficult than that of hydrogen in the hydrodeoxygenation over the Pd/ETS-10. In contrast, the vanillyl alcohol order (1.07) over the Pd/TiO<sub>2</sub> catalyst was higher than the order (0.81) over Pd/ETS-10 (Fig. 3), meaning stronger ability of Pd/ETS-10 than that of Pd/TiO<sub>2</sub> for the activation of the C–O bond.

Based on the aforementioned results, it can be concluded that better ability for the cleavage of the C–O bond without connection of the benzene ring in the substrate over Pd/ETS-10 could be related to the unique Pd–TiO<sub>x</sub> interfaces.

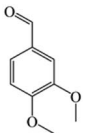
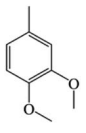
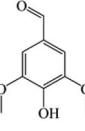
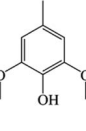
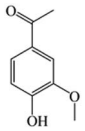
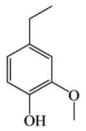
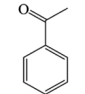
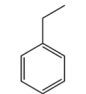
To study the properties of the unique Pd–TiO<sub>x</sub> interfaces, the interaction between the Pd nanoparticles and the TiO<sub>x</sub> nanowires in ETS-10 zeolite was characterized by UV-vis spectra because of the sensitive UV signals of TiO<sub>x</sub> species.<sup>23</sup> As shown in Fig. 4a, the ETS-10 sample shows an energy value of 2.98 eV. Loading Pd nanoparticles on ETS-10 makes the value shift to 3.06 eV (Fig. 4a), indicating strong interaction between the Pd nanoparticles and the TiO<sub>x</sub> nanowires in ETS-10. In contrast, the Pd/TiO<sub>2</sub> sample exhibited an energy value of 2.76 eV. This phenomenon indicated the different states of Pd–TiO<sub>x</sub> interfaces between the Pd/ETS-10 and Pd/TiO<sub>2</sub> catalysts. The different Pd–TiO<sub>x</sub> interfacial effects were further investigated by EPR spectra. As shown in Fig. 4b, the Pd/ETS-10 and Pd/TiO<sub>2</sub> samples showed two signals at *g* = 1.976 and 2.003, which can be related to the Ti<sup>3+</sup> species and the electrons trapped in the oxygen vacancies.<sup>21,34</sup> The intensities of the signals for Pd/ETS-10 were much stronger than those of Pd/TiO<sub>2</sub>, indicating that the loading of Pd nanoparticles on ETS-10 zeolite led to the formation of more Ti<sup>3+</sup> and oxygen vacancies in the catalyst, which are beneficial for the hydrodeoxygenation of biomass materials.

### 3.4 Substrate expansion and catalytic stability

The Pd/ETS-10 catalyst was also efficient for the hydrodeoxygenation of other lignin-derived substrates (Table 1). For example, after catalysis at 130 °C for 4 h, Pd/ETS-10 exhibited >99.9% veratraldehyde conversion and 78.0% 3,4-dimethoxytoluene yield (entry 1, Table 1); After catalysis at 140 °C for 4 h,



Table 1 Catalytic hydrodeoxygenation of various substrates over the Pd/ETS-10 catalyst<sup>a</sup>

Entry	Substrate	Product	Temperature (°C)	Time (h)	Conversion (%)	Yield (%)	Carbon balance (%)
1			130	4	>99.9	78.0	78.0
2			140	4	99.7	81.7	82.0
3			120	2	>99.9	88.5	88.5
4			130	4	99.0	75.0	76.0

<sup>a</sup> Reaction conditions: 6.5 mmol of substrate, 0.2 g of catalyst, 50 g of H<sub>2</sub>O, 1 MPa of H<sub>2</sub>, the reaction temperature and time are listed in the above table.

Pd/ETS-10 exhibited 99.7% syringaldehyde conversion and 81.7% 4-methylsyringol yield (entry 2, Table 1). In addition, the Pd/ETS-10 catalyst was also active in the hydrodeoxygenation of acetophenone. After catalysis at 130 °C for 4 h, Pd/ETS-10 exhibited 99.0% acetophenone conversion and 75.0% ethylbenzene yield (entry 4, Table 1). However, neither intermediate alcohol nor other compounds can be detected when the molecules in Table 1 were employed as the reaction substrates, implying carbon deposits occurred during the reactions. Therefore, the carbon balance data were also calculated, as shown in Table 1, and the Pd/ETS-10 catalyst exhibited carbon balance values of 78.0%, 82.0%, 88.5%, and 76.0%, when

veratraldehyde, syringaldehyde, apocynin, and acetophenone were applied as the substrates, respectively.

The Pd/ETS-10 sample is recyclable. To better evaluate the stability of Pd/ETS-10, we reduced the reaction time to 0.5 h, increased the S/C from 5 to 50, and used ethanol as a solvent to decrease the substrate conversion. As shown in Fig. 5, the TOF value of the fresh catalyst could reach 1.1 min<sup>-1</sup>. The activity of the catalyst gradually declined with increasing the recycles. After being used for 5 times, the TOF value was decreased to 0.62 min<sup>-1</sup> (Fig. 5). This phenomenon might result from coke deposition. After calcining the used catalyst at 350 °C for 1 h in flowing O<sub>2</sub> (30 mL min<sup>-1</sup>) to regenerate the catalyst, the Pd/ETS-10 catalyst exhibited a TOF value at 1.0 min<sup>-1</sup>, which was comparable to that (1.1 min<sup>-1</sup>) of the fresh one (Fig. 5). The hot filtration experiment was also performed to study the stability of the Pd/ETS-10 catalyst (Fig. S11<sup>†</sup>). After reaction for 15 min, the Pd/ETS-10 catalyst was filtered. The residue was allowed to react for another 30 min. Interestingly, the vanillin conversions at 15 and 45 min are equivalent (16%) within error (Fig. S11<sup>†</sup>), indicating that the active species in the Pd/ETS-10 catalyst were not leached during the reaction process.

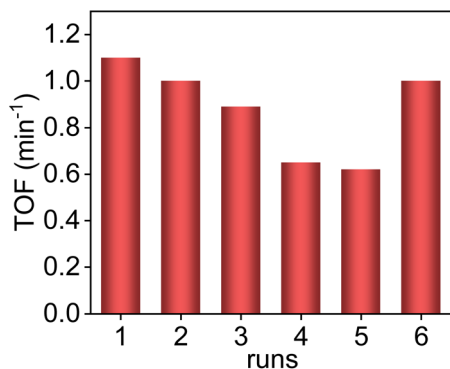


Fig. 5 Recyclability tests over the Pd/ETS-10 catalyst in the hydrodeoxygenation of vanillin. Reaction conditions: 1 g of vanillin, 0.02 g of catalyst, 20 ml of ethanol, 1 MPa of H<sub>2</sub>, 120 °C, and 0.5 h. After being used for 5 times, the catalyst was calcined at 350 °C for 1 h in flowing O<sub>2</sub> (30 mL min<sup>-1</sup>) to regenerate the catalyst.

## 4 Conclusions

In summary, we report the construction of interfaces between Pd nanoparticles and subnanoscale TiO<sub>x</sub> by loading Pd nanoparticles on the ETS-10 zeolite crystals. The unique Pd-TiO<sub>x</sub> interfaces in the Pd/ETS-10 sample are quite efficient for the selective removal of C=O bonds in the hydrodeoxygenation of vanillin and vanillin derivatives. Pd/ETS-10 exhibited >99.9% vanillin conversion and 95.2% 5-methylguaiaicol yield at 120 °C.



Kinetic studies, and characterization confirmed that the Pd-TiO<sub>x</sub> interfaces can effectively activate the C=O bonds in these biomass molecules. This work might be helpful for the development of efficient catalysts for the hydrodeoxygenation of biomass in the future.

## Author contributions

Jianbin Huang: conceptualization, methodology, investigation. Chang Zhou: conceptualization, methodology, investigation. Jian Zhang: conceptualization, methodology, writing – original draft. Hao Meng: methodology, investigation. Shiyao Lu: methodology, investigation. Feng-Shou Xiao: supervision, writing – review & editing.

## Conflicts of interest

There are no conflicts to declare.

## Acknowledgements

This work is supported by the National Key Research and Development Program of China (2018YFB0604801), and the National Natural Science Foundation of China (22002007 and 22272007).

## References

- 1 D. M. Alonso, S. G. Wettstein and J. A. Dumesic, *Chem. Soc. Rev.*, 2012, **41**, 8075–8098.
- 2 P. Sudarsanam, E. Peeters, E. V. Makshina, V. I. Parvulescu and B. F. Sels, *Chem. Soc. Rev.*, 2019, **48**, 2366–2421.
- 3 B. Ates, S. Koytepe, A. Ulu, C. Gurses and V. K. Thakur, *Chem. Rev.*, 2020, **120**, 9304–9362.
- 4 Z. Q. Ma, E. Troussard and J. A. van Bokhoven, *Appl. Catal., A*, 2012, **423**, 130–136.
- 5 K. Leiva, N. Martinez, C. Sepulveda, R. Garcia, C. A. Jimenez, D. Laurenti, M. Vrinat, C. Geantet, J. L. G. Fierro, I. T. Ghampson and N. Escalona, *Appl. Catal., A*, 2015, **490**, 71–79.
- 6 S. Crossley, J. Faria, M. Shen and D. E. Resasco, *Science*, 2010, **327**, 68–72.
- 7 J. Y. He, C. Zhao and J. A. Lercher, *J. Am. Chem. Soc.*, 2012, **134**, 20768–20775.
- 8 R. Weindl, R. Khare, L. Kovarik, A. Jentys, K. Reuter, H. Shi and J. A. Lercher, *Angew. Chem., Int. Ed.*, 2021, **60**, 9301–9305.
- 9 C. Wang, G. R. Wittreich, C. Lin, R. J. Huang, D. G. Vlachos and R. J. Gorte, *Catal. Lett.*, 2020, **150**, 913–921.
- 10 B. Boro, P. Koley, H. L. Tan, S. Biswas, R. Paul, S. Bhargava, W. Liu, B. M. Wong and J. Mondal, *ACS Appl. Nano Mater.*, 2022, **5**, 14706–14721.
- 11 J. L. Santos, P. Mäki-Arvela, J. Wärnä, A. Monzón, M. A. Centeno and D. Y. Murzin, *Appl. Catal., B*, 2020, **268**, 118425.
- 12 Z. Gao, Z. Zhou, M. Wang, N. Shang, W. Gao, X. Cheng, S. Gao, Y. Gao and C. Wang, *Fuel*, 2023, **334**, 126768.
- 13 R. Yangcheng, Y. Cui, S. Luo, J. Ran and J. Wang, *Microporous Mesoporous Mater.*, 2023, **350**, 112460.
- 14 J. Ran, R. YangCheng, Y. Cui and J. Wang, *ACS Sustain. Chem. Eng.*, 2022, **10**, 7277–7287.
- 15 H. H. Duan, J. C. Liu, M. Xu, Y. F. Zhao, X. L. Ma, J. C. Dong, X. S. Zheng, J. W. Zheng, C. S. Allen, M. Danaie, Y. K. Peng, T. Issariyakul, D. Chen, A. I. Kirkland, J. C. Buffet, J. Li, S. C. E. Tsang and D. O'Hare, *Nat. Catal.*, 2019, **2**, 1078–1087.
- 16 J. Zhang, B. W. Wang, E. Nikolla and J. W. Medlin, *Angew. Chem., Int. Ed.*, 2017, **56**, 6594–6598.
- 17 R. Y. Shu, B. Q. Lin, C. Wang, J. T. Zhang, Z. D. Cheng and Y. Chen, *Fuel*, 2019, **239**, 1083–1090.
- 18 J. K. Hedlund, D. C. Cronauer, G. Jacobs, A. J. Kropf, J. A. Libera, J. W. Elam, C. L. Marshall, V. R. R. Pendyala and B. H. Davis, *Catal. Lett.*, 2016, **146**, 525–539.
- 19 F. Lin, Y. Lu, K. A. Unocic, S. E. Habas, M. B. Griffin, J. A. Schaidle, H. M. Meyer III, Y. Wang and H. Wang, *ACS Catal.*, 2022, **12**, 465–480.
- 20 X. Q. Liu, J. Iocozzia, Y. Wang, X. Cui, Y. H. Chen, S. Q. Zhao, Z. Li and Z. Q. Lin, *Energy Environ. Sci.*, 2017, **10**, 402–434.
- 21 C. Y. Wang, Y. B. Li, C. B. Zhang, X. Y. Chen, C. L. Liu, W. Z. Weng, W. P. Shan and H. He, *Appl. Catal., B*, 2021, **282**, 119540.
- 22 M. W. Anderson, O. Terasaki, T. Ohsuna, A. Philippou, S. P. MacKay, A. Ferreira, J. Rocha and S. Lidin, *Nature*, 1994, **367**, 347–351.
- 23 L. Li, Y. Y. Cai, G. D. Li, X. Y. Mu, K. X. Wang and J. S. Chen, *Angew. Chem., Int. Ed.*, 2012, **51**, 4702–4706.
- 24 C. Casado, Z. Amghouz, J. R. Garcia, K. Boulahya, J. M. González-Calbet, C. Téllez and J. Coronas, *Mater. Res. Bull.*, 2009, **44**, 1225–1231.
- 25 Y. K. Krisnandi, E. E. Lachowski and R. F. Howe, *Chem. Mater.*, 2006, **18**, 928–933.
- 26 L. Kesavan, R. Tiruvalam, M. H. Ab Rahim, M. I. B. Saiman, D. I. Enache, R. L. Jenkins, N. Dimitratos, J. A. Lopez-Sanchez, S. H. Taylor, D. W. Knight, C. J. Kiely and G. J. Hutchings, *Science*, 2011, **331**, 195–199.
- 27 C. Williams, J. H. Carter, N. F. Dummer, Y. K. Chow, D. J. Morgan, S. Yacob, P. Serna, D. J. Willock, R. J. Meyer, S. H. Taylor and G. J. Hutchings, *ACS Catal.*, 2018, **8**, 2567–2576.
- 28 M. Xiang, X. J. Ni, X. F. Yi, A. M. Zheng, W. C. Wang, M. Y. He, J. Xiong, T. T. Liu, Y. L. Ma, P. Y. Zhu, X. Zheng and T. D. Tang, *ChemCatChem*, 2015, **7**, 521–525.
- 29 J. Ran, R. YangCheng, Y. Cui and J. Wang, *ACS Sustainable Chem. Eng.*, 2022, **10**, 7277–7287.
- 30 H. Huang, R. Zong and H. Li, *ACS Sustainable Chem. Eng.*, 2020, **8**, 15998–16009.
- 31 F. M. Zhang, S. Zheng, Q. Xiao, Y. J. Zhong, W. D. Zhu, A. Lin and S. El-Shall, *Green Chem.*, 2016, **18**, 2900–2908.
- 32 S. Deo, W. Medlin, E. Nikoll and M. J. Janik, *J. Catal.*, 2019, **377**, 28–40.
- 33 H. Jens, *Catalysis—A Practical Approach*, John Wiley & Sons Inc, 2006.
- 34 X. Y. Pan and Y. J. Xu, *ACS Appl. Mater. Interfaces*, 2014, **6**, 1879–1886.

